n-Butyllithium/*N*,*N*,*N'*,*N'*-Tetramethylethylenediamine-Mediated Ortholithiations of Aryl Oxazolines: Substrate-Dependent Mechanisms.

Scott T. Chadwick, Antonio Ramirez, Lekha Gupta, and David B. Collum*

Contribution from the Department of Chemistry and Chemical Biology
Baker Laboratory, Cornell University, Ithaca, New York 14853-1301

Supporting Information

Arenes **2**-**8** are known compounds that were prepared following described procedures:

Arene **2**: Wenker, H. *J. Am. Chem. Soc.* **1938**, *60*, 2152.
Arene **3**: Dawson, G. J.; Frost, C. G.; Martin, C. J.; Williams, J. M. J.; Coote, S. J. *Tetrahedron Lett.* **1993**, *34*, 7793.
Arene **4**: Meyers, A. I.; Mihelich, E. D. *J. Org. Chem.* **1975**, *40*, 3158.
Arene **5**: Shimano, M.; Meyers, A. I. *J. Am. Chem. Soc.* **1994**, *116*, 10815.
Arene **6**: Newman, M. S.; Kannan, R. *J. Org. Chem.* **1979**, *44*, 3388.
Arene **7**: Harris, T. D.; Neuschwander, B.; Boekelheide, V. *J. Org. Chem.* **1978**, *43*, 727.
Arene **8**: Witte, H.; Seeliger, W. *Angew. Chem., Int. Ed. Engl.* **1972**, *11*, 287.

Complete References

(30) Gaussian 03, Revision B.04, Frisch, M. J.; Trucks, G. W.; Schlegel, H. B.; Scuseria, G. E.; Robb, M. A.; Cheeseman, J. R.; Montgomery, Jr., J. A.; Vreven, T.; Kudin, K. N.; Burant, J. C.; Millam, J. M.; Iyengar, S. S.; Tomasi, J.; Barone, V.; Mennucci, B.; Cossi, M.; Scalmani, G.; Rega, N.; Petersson, G. A.; Nakatsuji, H.; Hada, M.; Ehara, M.; Toyota, K.; Fukuda, R.; Hasegawa, J.; Ishida, M.; Nakajima, T.; Honda, Y.; Kitao, O.; Nakai, H.; Klene, M.; Li, X.; Knox, J. E.; Hratchian, H. P.; Cross, J. B.; Bakken, V.; Adamo, C.; Jaramillo, J.; Gomperts, R.; Stratmann, R. E.; Yazyev, O.; Austin, A. J.; Cammi, R.; Pomelli, C.; Ochterski, J. W.; Ayala, P. Y.; Morokuma, K.; Voth, G. A.; Salvador, P.; Dannenberg, J. J.; Zakrzewski, V. G.; Dapprich, S.; Daniels, A. D.; Strain, M. C.; Farkas, O.; Malick, D. K.; Rabuck, A. D.; Raghavachari, K.; Foresman, J. B.; Ortiz, J. V.; Cui, Q.; Baboul, A. G.; Clifford, S.; Cioslowski, J.; Stefanov, B. B.; Liu, G.; Liashenko, A.; Piskorz, P.; Komaromi, I.; Martin, R. L.; Fox, D. J.; Keith, T.; Al-Laham, M. A.; Peng, C. Y.; Nanayakkara, A.; Challacombe, M.; Gill, P. M. W.; Johnson, B.; Chen, W.; Wong, M. W.; Gonzalez, C.; and Pople, J. A.; Gaussian, Inc., Wallingford CT, 2004.

36 (c) Pratt, L. M.; Newman, A.; St. Cyr, J.; Johnson, H.; Miles, B.; Lattier, A.; Austin, E.; Henderson, S.; Hershey, B.; Lin, M.; Balamraju, Y.; Sammonds, L.; Cheramie, J.; Karnes, J.; Hymel, E.; Woodford, B.; Carter, C. *J. Org. Chem.* **2003**, *68*, 6387

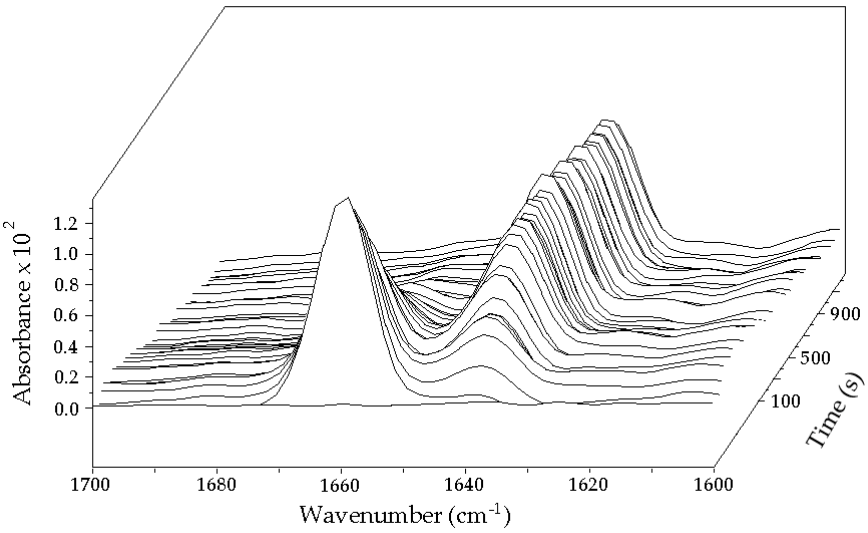

I. Representative in situ IR spectroscopic analysis of the ortholithiation of arene **8** (0.02 M) by *n*-BuLi (0.5 M) in TMEDA (0.5 M) and pentane cosolvent at -40 °C. The IR absorbance at 1660 cm^{-1} corresponds to **8**, whereas the absorbance at 1635 cm^{-1} corresponds to its lithiated form **8**-Li.

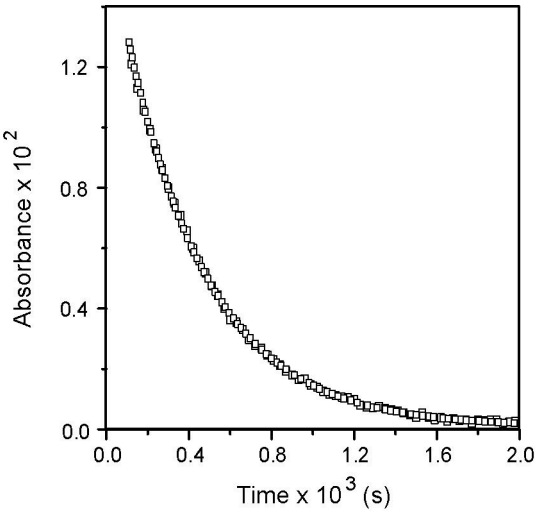

II. Loss of arene **8** for the ortholithiation in Section I.

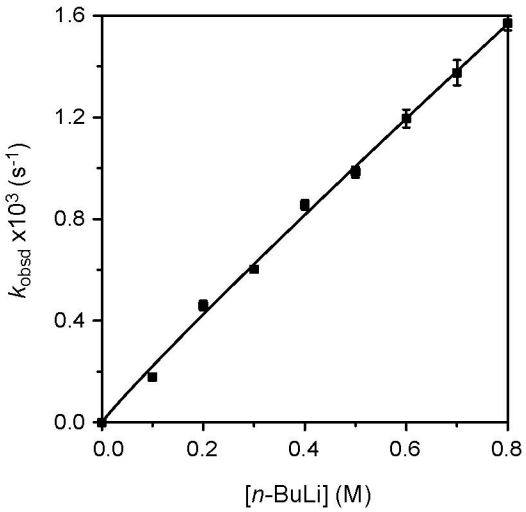

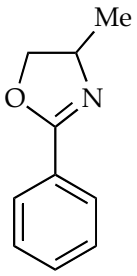

3

III. Plot of k_{obsd} vs [*n*-BuLi] in TMEDA (0.5 M) and pentane cosolvent for the ortholithiation of 4-methyl-2-phenyl-4,5-dihydrooxazole (**3**, 0.02 M) at -78 ˚C. The curve depicts an unweighted least-squares fit to $k_{obsd} = k[n\text{-BuLi}]^n$ (k = (1.93 ± 0.01) x 10^{-3}, n = 0.94 ± 0.03).

[*n*-BuLi] (M)	$k_{obsd}1$ (s^{-1})	$k_{obsd}2$ (s^{-1})	k_{obsd}av (s^{-1})
0.1	0.000183 ± 6E-6	0.000175 ± 8E-6	0.000179 ± 5E-6
0.2	0.000473 ± 3E-6	0.00045 ± 1E-5	0.00046 ± 2E-5
0.3	0.000593 ± 8E-6	0.000612 ± 8E-6	0.00060 ± 1E-5
0.4	0.000869 ± 8E-6	0.000843 ± 7E-6	0.00086 ± 2E-5
0.5	0.00097 ± 1E-5	0.00100 ± 2E-5	0.00098 ± 2E-5
0.6	0.00117 ± 2E-6	0.00122 ± 9E-6	0.00119 ± 3E-5
0.7	0.00134 ± 5E-5	0.00141 ± 6E-6	0.00137 ± 5E-5
0.8	0.00159 ± 7E-5	0.00155 ± 4E-6	0.00157 ± 3E-5

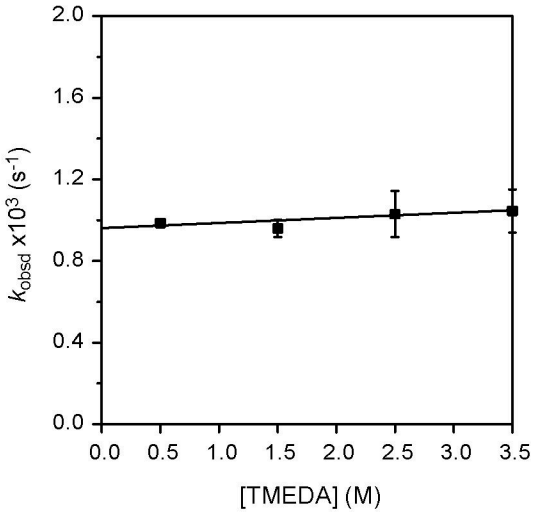

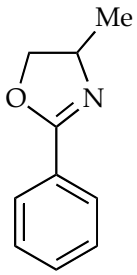

3

IV. Plot of k_{obsd} vs [TMEDA] in pentane cosolvent for the ortholithiation of 4-methyl-2-phenyl-4,5-dihydrooxazole (**3**, 0.02 M) by *n*-BuLi (0.5 M) at -78 ˚C. The curve depicts an unweighted least-squares fit to $k_{obsd} = k$[TMEDA] + k' (k = (2 $\pm$ 1) x 10^{-5}, k' = (9.5 $\pm$ 0.3) x 10^{-4}).

[TMEDA] (M)	$k_{obsd}1$ (s^{-1})	$k_{obsd}2$ (s^{-1})	k_{obsd}av (s^{-1})
0.5	0.00097 $\pm$ 1E-5	0.00100 $\pm$ 2E-5	0.00098 $\pm$ 2E-5
1.5	0.00099 $\pm$ 9E-5	0.00093 $\pm$ 7E-5	0.00096 $\pm$ 4E-5
2.5	0.00111 $\pm$ 1E-5	0.00095 $\pm$ 8E-5	0.0011 $\pm$ 1E-4
3.5	0.00097 $\pm$ 8E-5	0.00112 $\pm$ 9E-5	0.0010 $\pm$ 1E-5

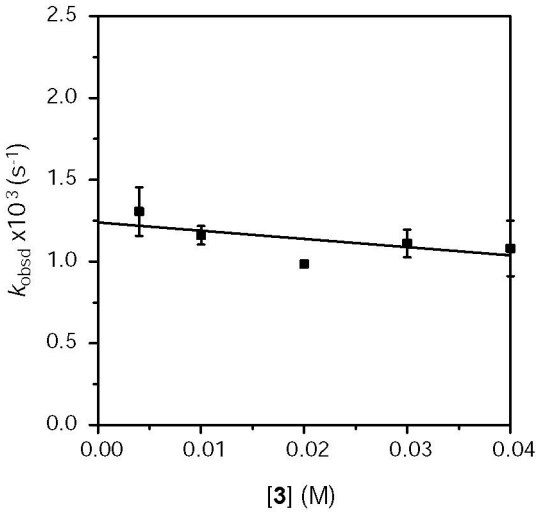

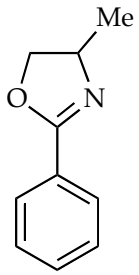

3

V. Plot of k_{obsd} vs [**3**] in TMEDA (0.5 M) and pentane cosolvent for the ortholithiation of 4-methyl-2-phenyl-4,5-dihydrooxazole (**3**) by *n*-BuLi (0.5 M) at -78 °C. The curve depicts an unweighted least-squares fit to $k_{obsd} = k[\mathbf{3}] + k'$ ($k = (5 \pm 4) \times 10^{-3}$, $k' = (1.2 \pm 0.1) \times 10^{-3}$).

[**3**] (M)	$k_{obsd}1$ (s^{-1})	$k_{obsd}2$ (s^{-1})	k_{obsd}av (s^{-1})
0.004	0.00141 ± 7E-5	0.0012 ± 1E-4	0.0013 ± 1E-4
0.01	0.00112 ± 2E-5	0.00120 ± 8E-5	0.00116 ± 6E-5
0.02	0.00097 ± 1E-5	0.00110 ± 9E-5	0.00098 ± 2E-5
0.03	0.00117 ± 1E-5	0.00105 ± 2E-5	0.00111 ± 8E-5
0.04	0.00096 ± 1E-5	0.0012 ± 1E-4	0.0011 ± 2E-4

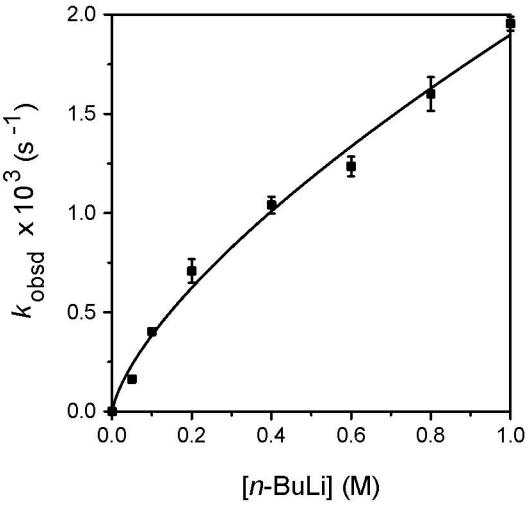

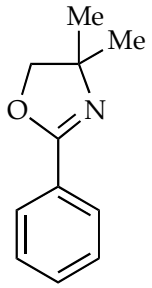

4

VI. Plot of k_{obsd} vs [*n*-BuLi] in TMEDA (0.5 M) and pentane cosolvent for the ortholithiation of 2-phenyl-4,4-dimethyl-4,5-dihydrooxazole (**4**, 0.02 M) at -40 ˚C. The curve depicts an unweighted least-squares fit to $k_{obsd} = k[n\text{-BuLi}]^n$ (k = (1.90 ± 0.05) x 10^{-3}, n = 0.69 ± 0.04).

[*n*-BuLi] (M)	$k_{obsd}1$ (s^{-1})	$k_{obsd}2$ (s^{-1})	k_{obsd}av (s^{-1})
0.05	0.00017 ± 1E-5	0.00015 ± 1E-5	0.00016 ± 1E-5
0.10	0.00041 ± 2E-5	0.00039 ± 1E-5	0.00040 ± 1E-5
0.20	0.00066 ± 2E-5	0.00075 ± 3E-5	0.00071 ± 6E-5
0.40	0.00101 ± 5E-5	0.00107 ± 5E-5	0.00104 ± 4E-5
0.60	0.00127 ± 6E-5	0.00120 ± 5E-5	0.00123 ± 5E-5
0.80	0.00166 ± 7E-5	0.00154 ± 2E-5	0.00160 ± 8E-5
1.00	0.00193 ± 7E-5	0.00198 ± 8E-5	0.00195 ± 3E-5

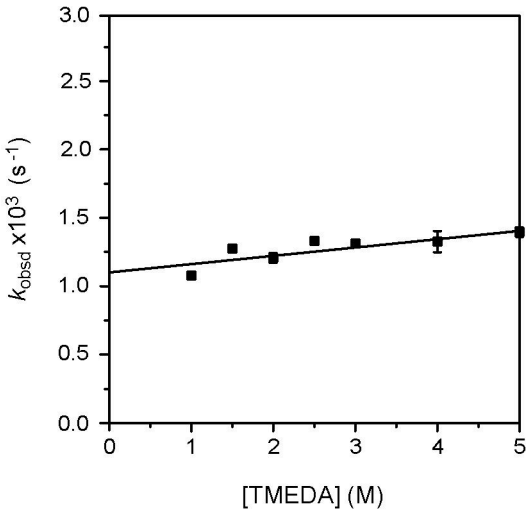

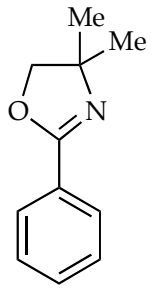

4

VII. Plot of k_{obsd} vs [TMEDA] in pentane cosolvent for the ortholithiation of 2-phenyl-4,4-dimethyl-4,5-dihydrooxazole (**4**, 0.02 M) by *n*-BuLi (0.5 M) at -40 °C. The curve depicts the result of an unweighted least-squares fit to $k_{obsd} = k[\text{TMEDA}] + k'$ ($k = (6 \pm 2)$ x 10^{-5}, $k' = (11.2 \pm 0.6)$ x 10^{-4}).

[TMEDA] (M)	$k_{obsd}1$ (s^{-1})	$k_{obsd}2$ (s^{-1})	k_{obsd}av (s^{-1})
1.00	0.00107 ± 1E-5	0.00110 ± 1E-5	0.00108 ± 2E-5
1.50	0.00130 ± 2E-5	0.00127 ± 7E-5	0.00128 ± 2E-5
2.00	0.00119 ± 2E-5	0.00124 ± 3E-5	0.00121 ± 3E-5
2.50	0.00135 ± 5E-5	0.00133 ± 8E-5	0.00134 ± 1E-5
3.00	0.00134 ± 6E-5	0.00130 ± 5E-5	0.00132 ± 3E-5
4.00	0.00139 ± 7E-5	0.00128 ± 2E-5	0.0133 ± 1E-4
5.00	0.00138 ± 7E-5	0.00143 ± 8E-5	0.00140 ± 3E-5

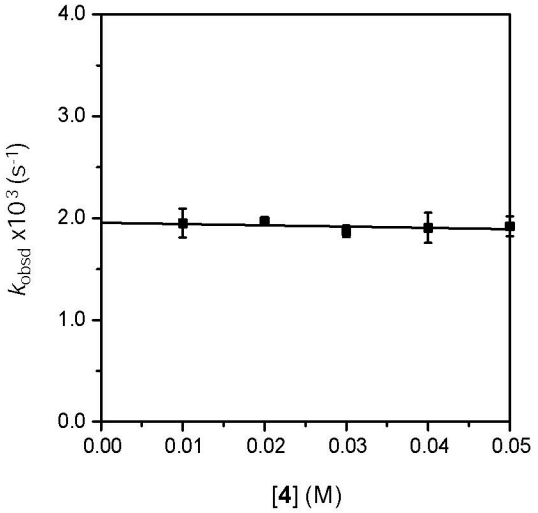

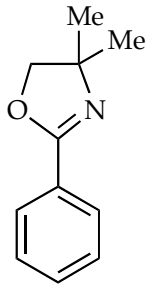

4

VIII. Plot of k_{obsd} vs [**4**] in TMEDA (0.5 M) and pentane cosolvent for the ortholithiation of 2-phenyl-4,4-dimethyl-4,5-dihydrooxazole (**4**) by *n*-BuLi (1.0 M) at -40 °C. The curve depicts an unweighted least-squares fit to $k_{obsd} = k[\mathbf{4}] + k'$ ($k = (1 \pm 1) \times 10^{-3}$, $k' = (19.6 \pm 0.4) \times 10^{-5}$).

[**4**] (M)	$k_{obsd}1$ (s^{-1})	$k_{obsd}2$ (s^{-1})	k_{obsd}av (s^{-1})
0.01	0.00205 ± 8E-5	0.00185 ± 9E-5	0.0019 ± 1E-4
0.02	0.0020 ± 1E-4	0.00194 + 8E-5	0.00197 ± 4E-5
0.03	0.00191 ± 8E-5	0.00183 ± 7E-5	0.00187 ± 6E-5
0.04	0.0018 ± 1E-4	0.00201 ± 8E-5	0.0019 ± 1E-4
0.05	0.00199 ± 6E-5	0.00185 ± 8E-5	0.0019 ± 1E-4

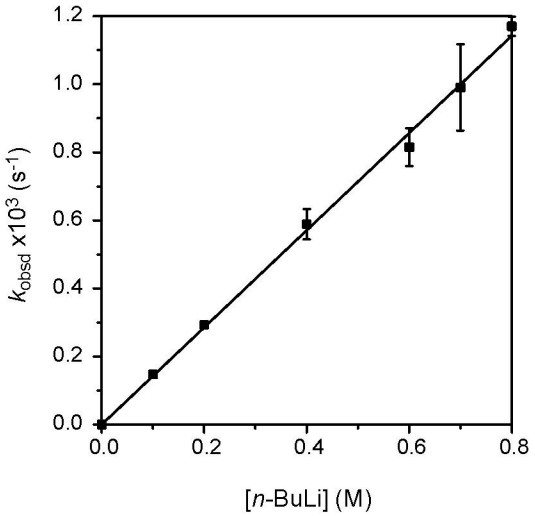

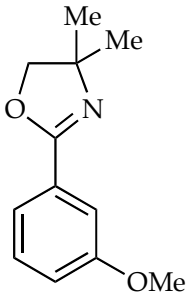

5

IX. Plot of k_{obsd} vs [*n*-BuLi] in TMEDA (0.5 M) and pentane cosolvent for the ortholithiation of 2-(3-methoxyphenyl)-4,4-dimethyl-4,5-dihydrooxazole (**5**, 0.02 M) at -78 °C. The curve depicts an unweighted least-squares fit to $k_{obsd} = k[n\text{-BuLi}]^n$ (k = 1.42 ± 0.03 x 10^{-3}, n = 1.00 ± 0.04).

[*n*-BuLi] (M)	$k_{obsd}1$ (s^{-1})	$k_{obsd}2$ (s^{-1})	k_{obsd}av (s^{-1})
0.1	0.000144 ± 1E-6	0.00015 ± 4E-5	0.000147 ± 5E-6
0.2	0.000299 ± 1E-6	0.000287 ± 9E-6	0.000293 ± 8E-6
0.4	0.000557 ± 8E-6	0.000620 ± 8E-6	0.00059 ± 4E-5
0.6	0.000776 ± 7E-6	0.000854 ± 9E-6	0.00081 ± 5E-5
0.7	0.000901 ± 7E-6	0.00108 ± 5E-5	0.0010 ± 1E-4
0.8	0.00115 ± 1E-5	0.00119 ± 6E-5	0.00117 ± 3E-5

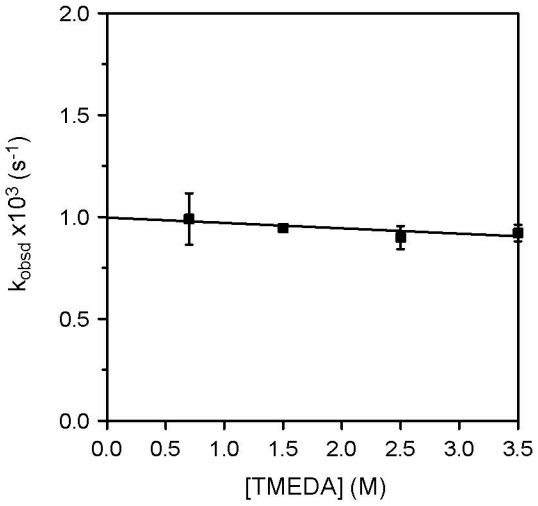

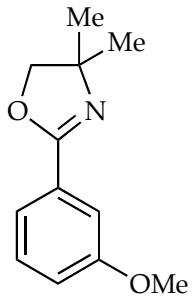

5

X. Plot of k_{obsd} vs [TMEDA] in pentane cosolvent for the ortholithiation of 2-(3-methoxyphenyl)-4,4-dimethyl-4,5-dihydrooxazole (**5**, 0.02 M) by *n*-BuLi (0.7 M) at -78 °C. The curve depicts an unweighted least-squares fit to $k_{obsd} = k$[TMEDA] + k' (k = (-3 ± 1) x 10^{-5}, k' = (9.9 ± 0.3) x 10^{-4}).

[TMEDA] (M)	k_{obsd}1 (s^{-1})	k_{obsd}2 (s^{-1})	k_{obsd}av (s^{-1})
0.7	0.000901 ± 7E-6	0.00108 ± 5E-5	0.0010 ± 1E-4
1.5	0.00096 ± 1E-5	0.000932 ± 6E-6	0.00095 ± 2E-5
2.5	0.00086 ± 2E-5	0.00094 ± 7E-5	0.00090 ± 6E-5
3.5	0.00095 ± 2E-5	0.00089 ± 9E-5	0.00092 ± 4E-5

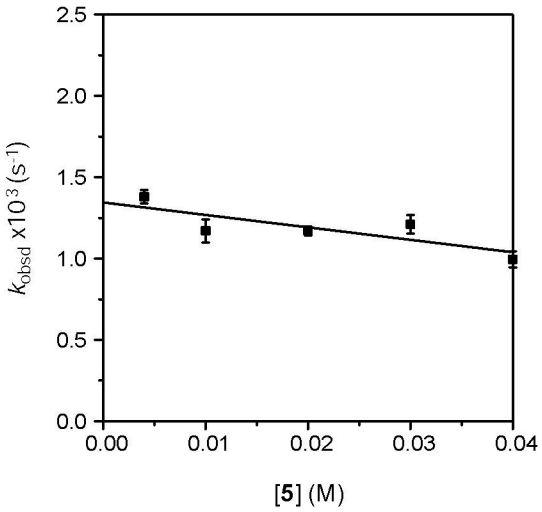

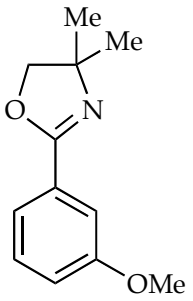

5

XI. Plot of k_{obsd} vs [**5**] in TMEDA (0.5 M) and pentane cosolvent for the ortholithiation of 2-(3-methoxyphenyl)-4,4-dimethyl-4,5-dihydrooxazole (**5**) by *n*-BuLi (0.8 M) at -78 °C. The curve depicts an unweighted least-squares fit to $k_{obsd} = k[\mathbf{5}] + k'$ (k = (-0.8 ± 0.3) x 10^{-2}, k' = (1.3 ± 0.1) x 10^{-3}).

[**5**] (M)	$k_{obsd}1$ (s^{-1})	$k_{obsd}2$ (s^{-1})	k_{obsd}av (s^{-1})
0.004	0.00141 ± 7E-5	0.00135 ± 8E-5	0.00138 ± 4E-5
0.01	0.00112 ± 2E-5	0.0012 ± 1E-4	0.00117 ± 7E-5
0.02	0.00115 ± 1E-5	0.00119 ± 6E-5	0.00117 ± 3E-5
0.03	0.00117 ± 1E-5	0.00125 ± 7E-5	0.00121 ± 6E-5
0.04	0.00096 ± 1E-5	0.00103 ± 9E-5	0.00099 ± 5E-5

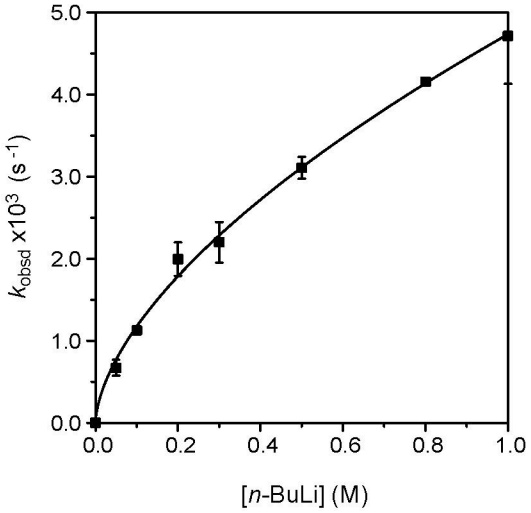

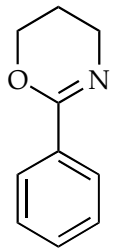

8

XII. Plot of k_{obsd} vs [*n*-BuLi] in TMEDA (0.5 M) and pentane cosolvent for the ortholithiation of 2-phenyl-5,6-dihydro-4*H*-1,3-oxazine (**8**, 0.02 M) at -40 °C. The curve depicts an unweighted least-squares fit to $k_{obsd} = k[n\text{-BuLi}]^n$ (k = (3.8 ± 0.1) x 10^{-3}, n = 0.60 ± 0.02).

[*n*-BuLi] (M)	$k_{obsd}1$ (s^{-1})	$k_{obsd}2$ (s^{-1})	k_{obsd}av (s^{-1})
0.05	0.00059 ± 6E-5	0.00048 ± 5E-5	0.00053 ± 7E-5
0.10	0.0009 ± 1E-4	0.00090 ± 6E-5	0.00091 ± 2E-5
0.20	0.00148 ± 2E-5	0.00171 ± 3E-5	0.0016 ± 2E-4
0.30	0.0019 ± 1E-4	0.00162 ± 8E-5	0.0018 ± 2E-4
0.50	0.00241 + 7E-5	0.00256 + 6E-5	0.0025 + 1E-4
0.80	0.00335 ± 8E-5	0.0033 ± 1E-4	0.00334 ± 1E-5
1.00	0.00410 ± 8E-5	0.00344 ± 8E-5	0.0038 ± 4E-4

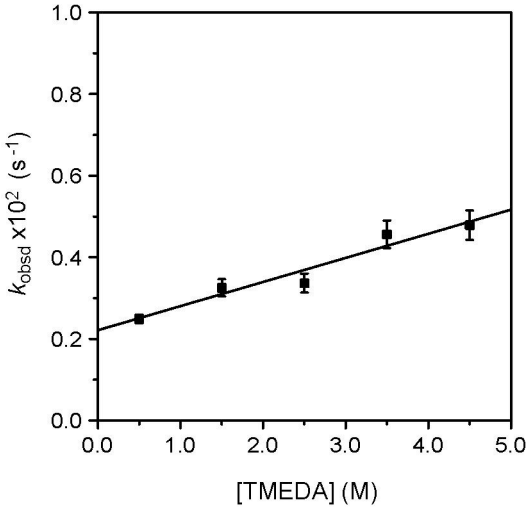

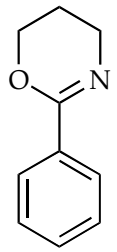

8

XIII. Plot of k_{obsd} vs [TMEDA] in pentane cosolvent for the ortholithiation of 2-phenyl-5,6-dihydro-4*H*-1,3-oxazine (**8**, 0.02 M) by *n*-BuLi (0.5 M) at -40 °C. The curve depicts an unweighted least-squares fit to $k_{obsd} = k$[TMEDA] + k' (k = (5.9 ± 0.8) x 10^{-4}, k' = (2.2 ± 0.2) x 10^{-3}).

[TMEDA] (M)	$k_{obsd}1$ (s^{-1})	$k_{obsd}2$ (s^{-1})	k_{obsd}av (s^{-1})
0.5	0.00241 ± 7E-5	0.00256 ± 6E-5	0.0025 ± 1E-4
1.5	0.0034 ± 2E-4	0.00310 ± 8E-5	0.0032 ± 2E-4
2.5	0.0032 ± 1E-4	0.0035 ± 1E-4	0.0034 ± 2E-4
3.5	0.0048 ± 2E-4	0.0043 ± 1E-4	0.0046 ± 3E-4
4.5	0.00504 ± 9E-5	0.00453 ± 9E-5	0.0048 ± 4E-4

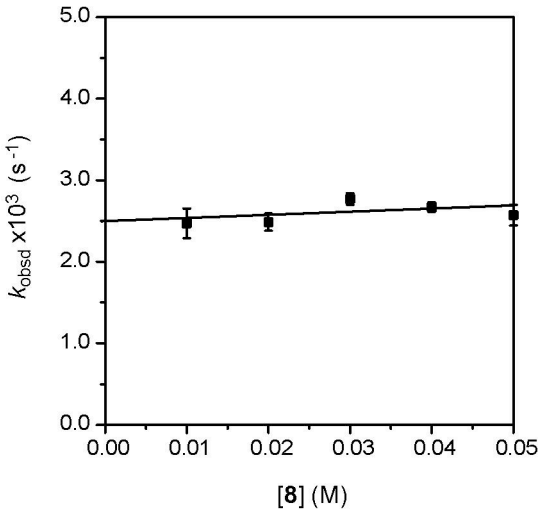

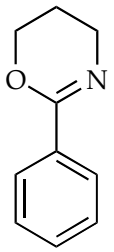

8

XIV. Plot of k_{obsd} vs [**8**] in TMEDA (0.5 M) and pentane cosolvent for the ortholithiation of 2-phenyl-5,6-dihydro-4*H*-1,3-oxazine (**8**) by *n*-BuLi (0.5 M) at -40 ˚C. The curve depicts an unweighted least-squares fit to $k_{obsd} = k[\mathbf{8}] + k'$ ($k = (4 \pm 4) \times 10^{-3}$, $k' = (2.5 \pm 0.1) \times 10^{-3}$).

[**8**] (M)	$k_{obsd}1$ (s^{-1})	$k_{obsd}2$ (s^{-1})	k_{obsd}av (s^{-1})
0.01	0.0026 ± 3E-4	0.00234 ± 8E-5	0.0025 ± 2E-4
0.02	0.00241 ± 7E-5	0.00256 ± 6E-5	0.0025 ± 1E-4
0.03	0.00272 ± 4E-5	0.00282 ± 6E-5	0.00277 ± 7E-5
0.04	0.00271 ± 3E-5	0.00263 ± 9E-5	0.00267 ± 6E-5
0.05	0.00266 ± 2E-5	0.00248 ± 6E-5	0.0026 ± 1E-4

XV. DFT Computational Studies

A. Optimized geometries and free energies (*G*, Hartrees) of reactants.[a]

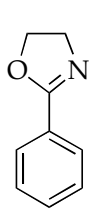

I

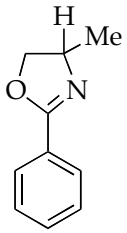

II

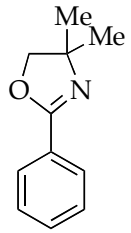

III

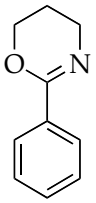

IV

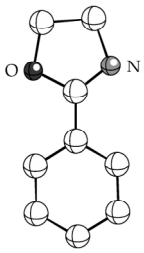

-478.21601

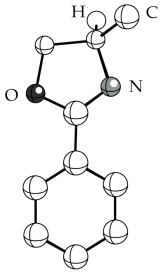

-517.50787

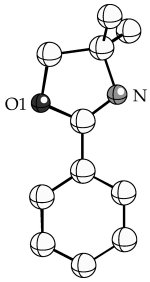

-556.79909

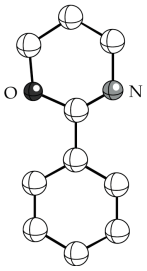

-517.50098

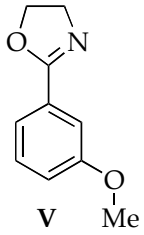

V

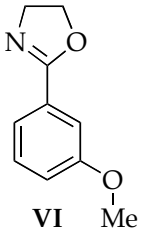

VI

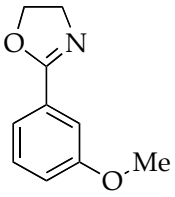

VII

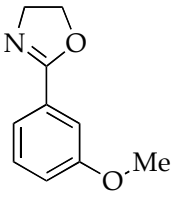

VIII

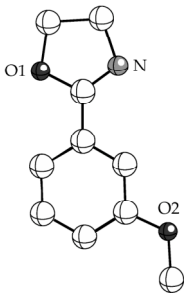

-592.70888

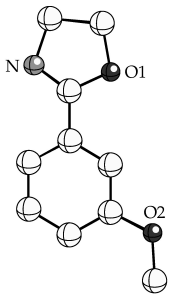

-592.70893

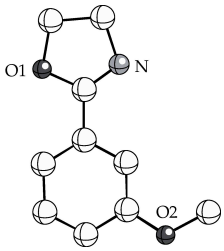

-592.70983

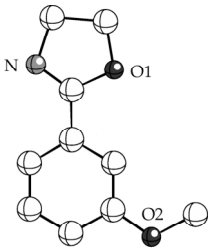

-592.70922

[a] Only selected hydrogens shown for clarity.

XV (*Continued*).

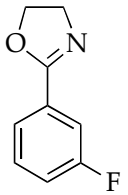

IX

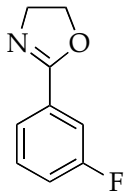

X

XI

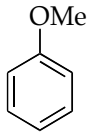

XII

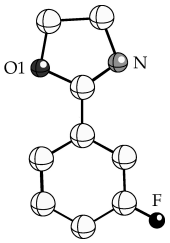

-577.45851

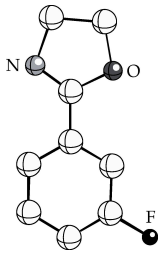

-577.45874

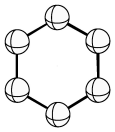

-232.17539

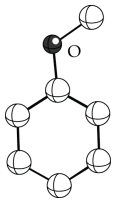

-346.66873

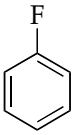

XIII

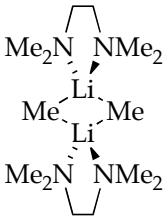

XIV

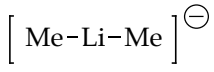

XV

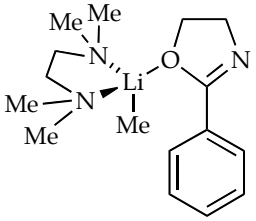

XVI

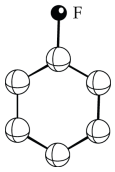

-331.41852

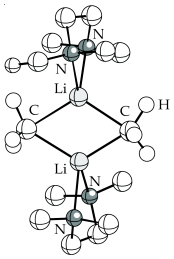

$(MeLi)_2TMEDA_2$
-789.97249

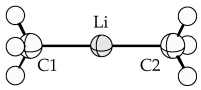

$[Me_2Li]^-$
-87.28524

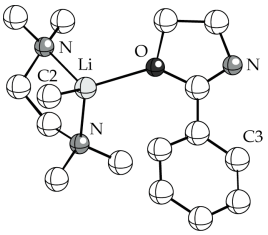

-873.17992

ΔG $^{+}Li(TMEDA)_2$ = -702.55451. ΔG $[Me_2Li]$ $^{-+}Li(TMEDA)_2$ = -789.92639. ΔG TMEDA = -347.558487.

XV (*Continued*).

B. Optimized geometries and free energies (*G*, Hartrees) of triple-ion-based transition structures.[a] $\Delta G_{ti}^{\ddagger}$'s corresponding to eq 15 shown in parentheses.

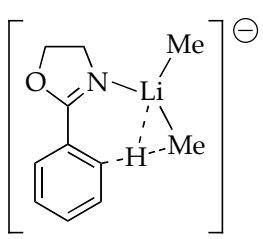

A

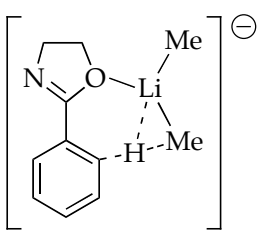

B

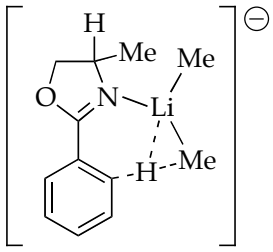

C

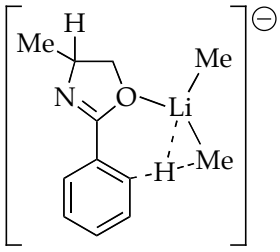

D

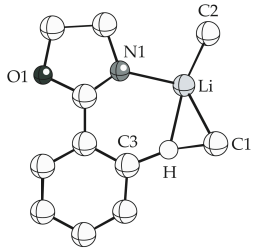

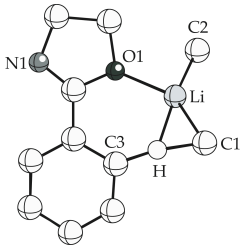

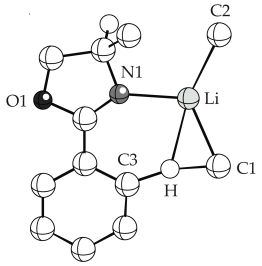

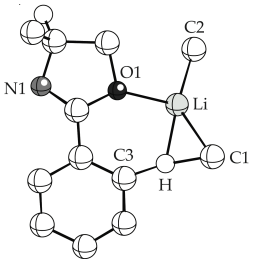

-565.47472 (+16.6) -565.47271 (+17.9) -604.76543 (+17.4) -604.76570 (+17.2)

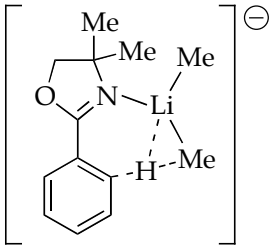

E

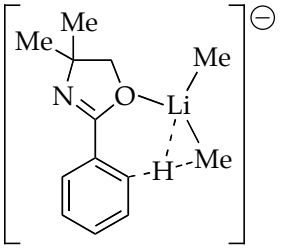

F

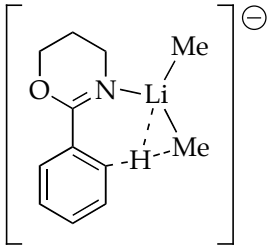

G

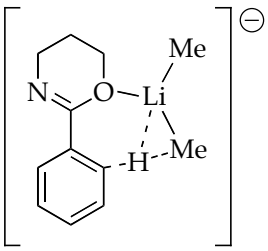

H

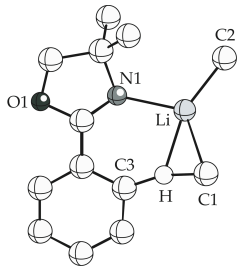

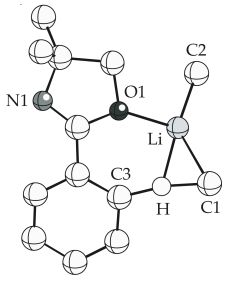

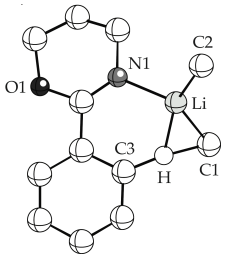

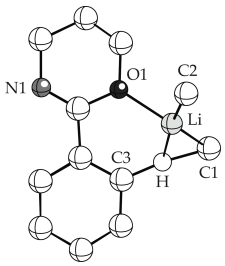

-644.05558 (+18.0) -644.05590 (+17.8) -604.75629 (+18.8) -604.75613 (+18.9)

[a] Only selected hydrogens shown for clarity.

XV (*Continued*).

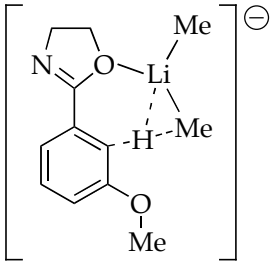

J

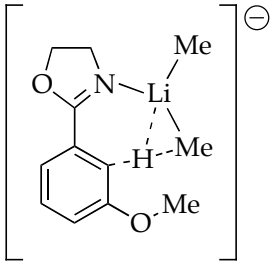

K

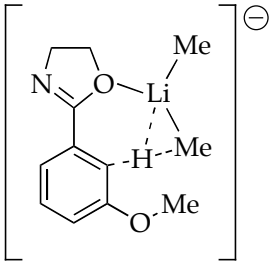

L

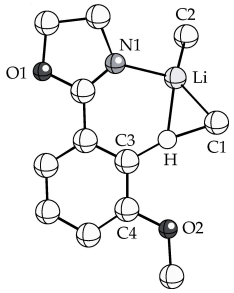

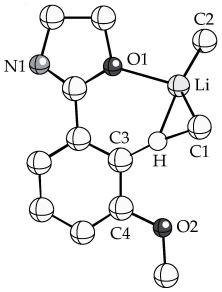

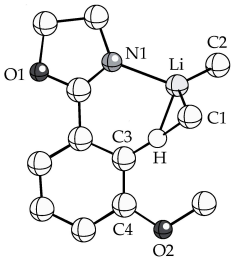

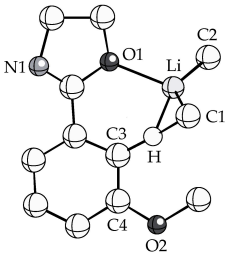

-679.96604 (+18.2)

-679.96464 (+19.1)

-679.97101 (+15.1)

-679.97018 (+15.6)

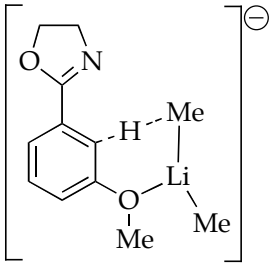

M

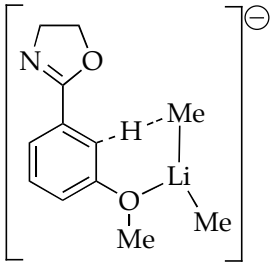

N

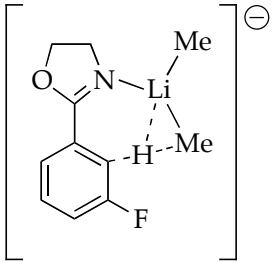

O

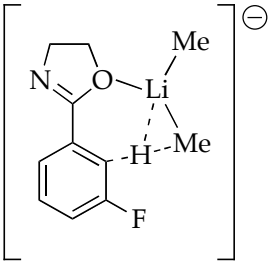

P

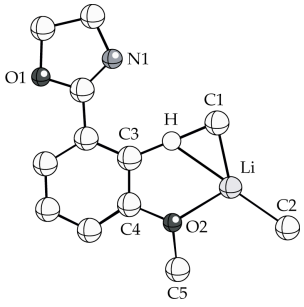

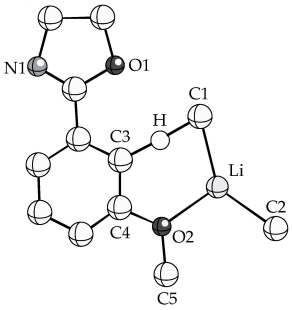

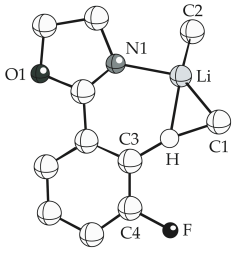

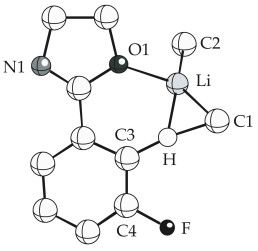

-679.96201 (+20.7)

-679.96556 (+18.5)

-664.72438 (+12.3)

-664.72352 (+12.8)

XV (*Continued*).

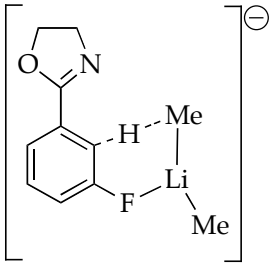

Q

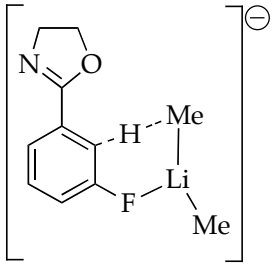

R

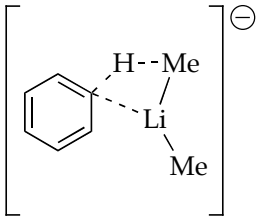

S

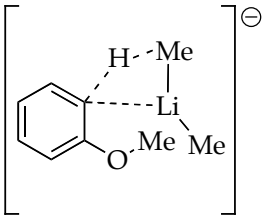

T

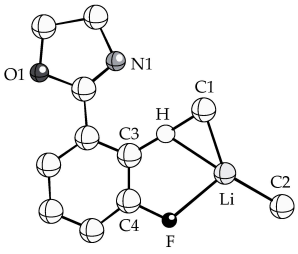

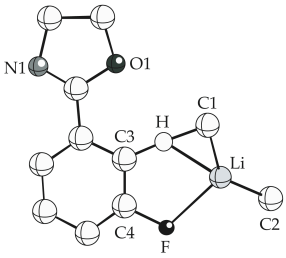

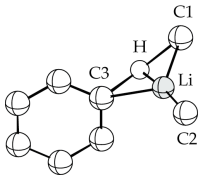

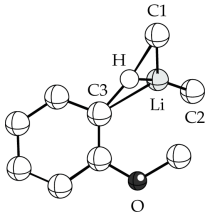

-664.71807 (+16.2) -664.72077 (+14.6) -319.42640 (+21.5) -433.92515[b] (+18.1)

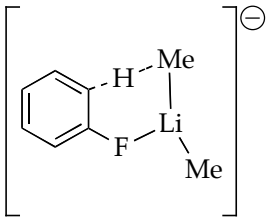

U

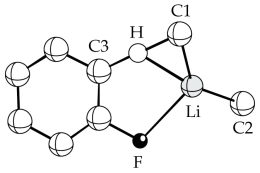

-418.67993 (+14.9)

XV (*Continued*).

C. Optimized geometries and free energies (*G*, Hartrees) of monomer-based transition structures.[a] $\Delta G_m^{\ddagger}$'s corresponding to eq 9 shown in parentheses.

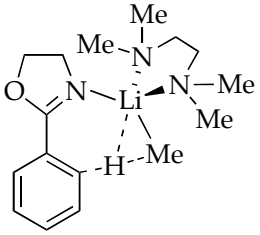

V

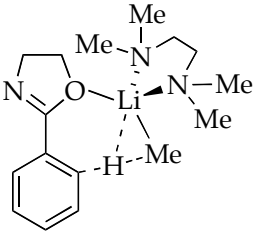

W

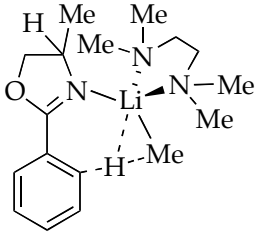

X

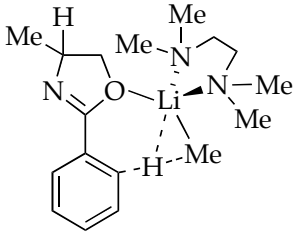

Y

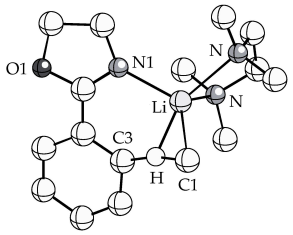

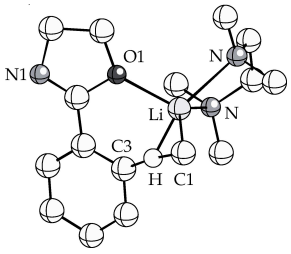

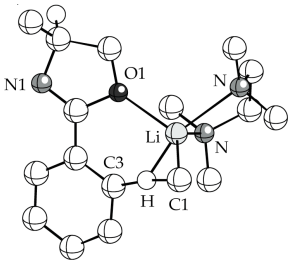

-873.16525 (+23.2) -873.15609 (+28.9) not found -912.44787 (+29.0)

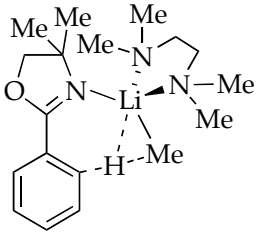

Z

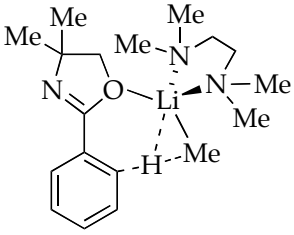

AA

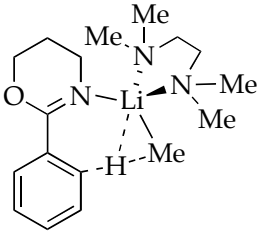

BB

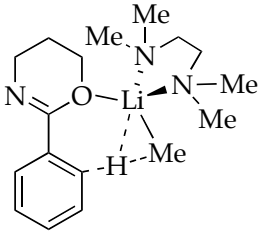

CC

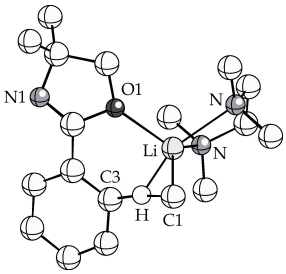

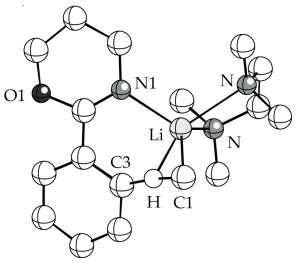

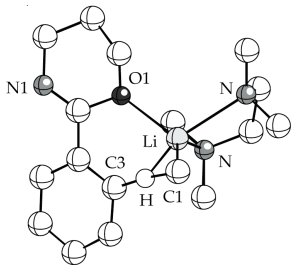

not found -951.73864 (+29.3) -912.44625 (+25.7) -912.43785 (+31.0)

[a] Only selected hydrogens shown for clarity.

XV (*Continued*).

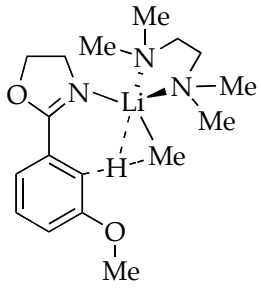

DD

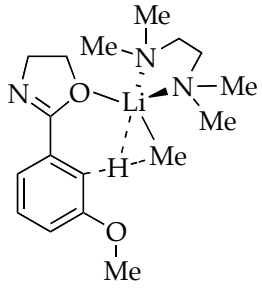

EE

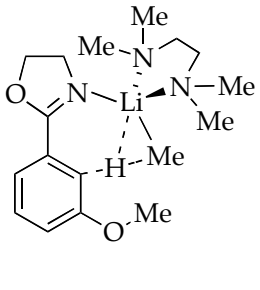

FF

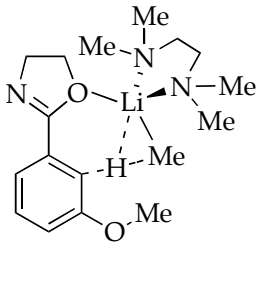

GG

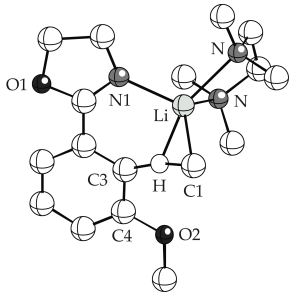

-987.65933 (+23.0)

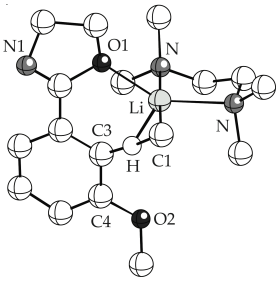

-987.64786 (+30.2)

not found

not found

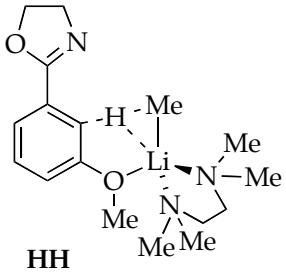

HH

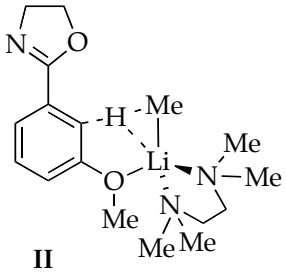

II

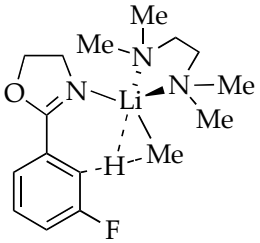

JJ

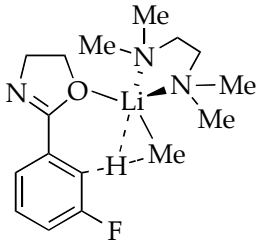

KK

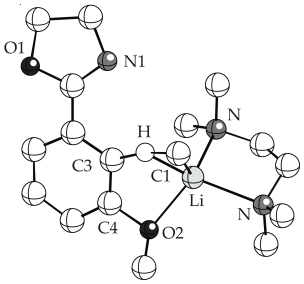

-987.65276 (+27.2)

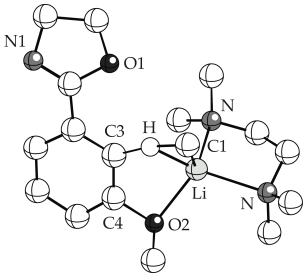

-987.65201 (+27.7)

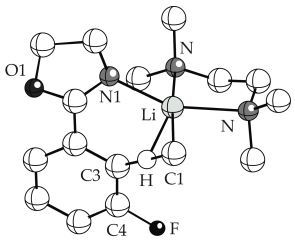

-972.40875 (+22.7)

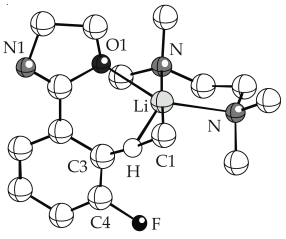

-972.40214 (+26.8)

XV (*Continued*).

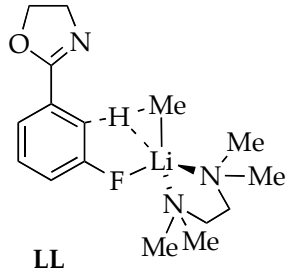

LL

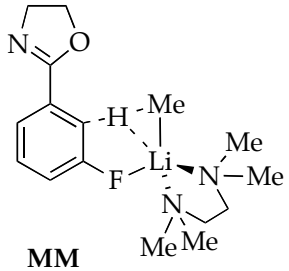

MM

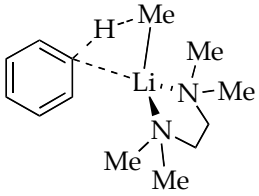

NN

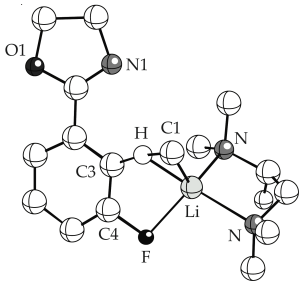

-972.40911 (+22.4)

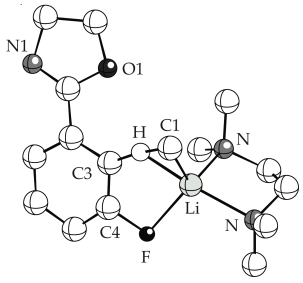

-972.40979 (+22.0)

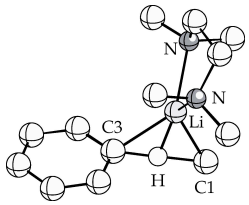

-627.11261 (+30.8)

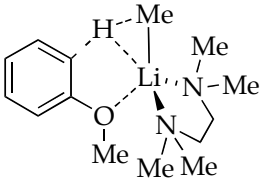

OO

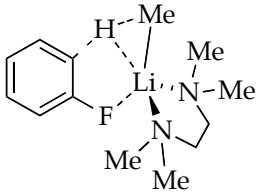

PP

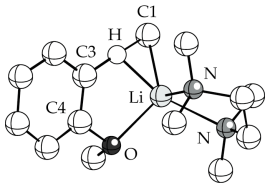

-741.61208 (+26.9)[b]

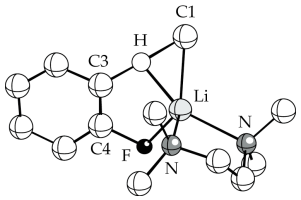

-726.37016 (+21.7)

[b]Most stable anti-MeO conformer shown, ($\Delta G_m^{\ddagger}$ syn-MeO = -741.607200, +30.0 kcal/mol).

XV (*Continued*).

D. Optimized geometries and free energies (*G*, Hartrees) of dimer-based transition structures.[a] $\Delta G_d^{\ddagger}$'s associated to Chart 2 and eq 12 shown in parentheses.

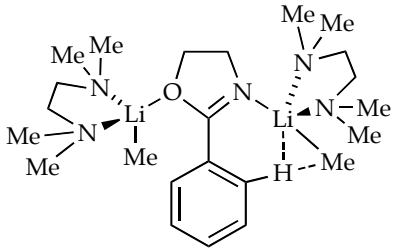

QQ

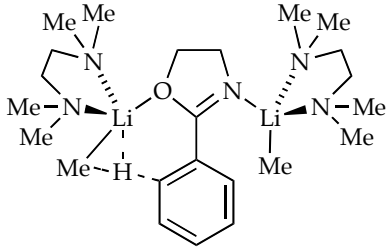

RR

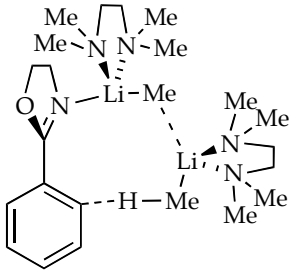

SS

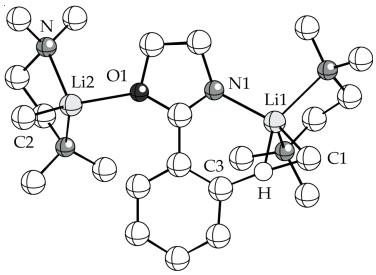

-1268.12395 (+40.5)

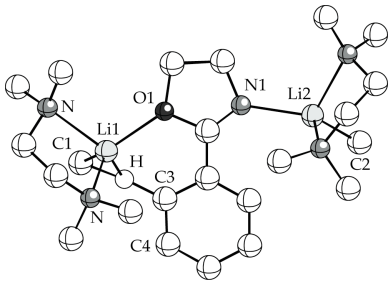

-1268.12072 (+42.5)

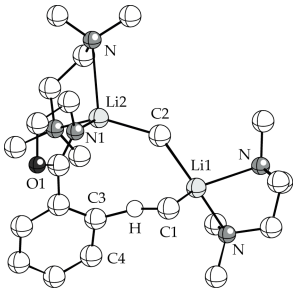

-1268.11678 (+45.0)

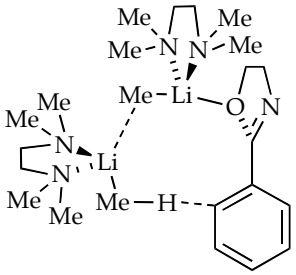

TT

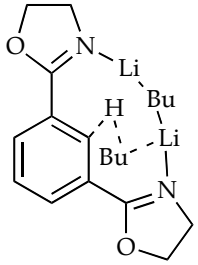

UU

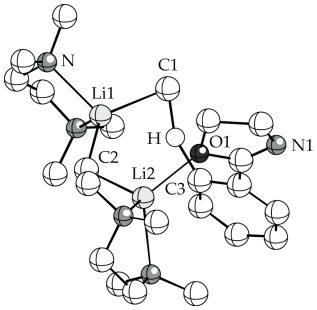

-1268.11502 (+46.1)

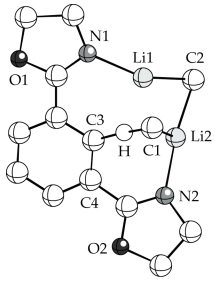

-819.08969

[a] Only selected hydrogens shown for clarity.

XVI. Selected bond lengths (Å) and angles (deg) for triple-ion-based transition structures **A**-**U**.[a]

bond/angle	**A**	**B**	**C**	**D**	**E**	**F**	**G**	**H**	**I**	**J**
Li-N	2.10	---	2.10	---	2.10	---	2.12	---	2.09	---
Li-O	---	2.10	---	2.10	---	2.10	---	2.13	---	2.10
Li-C3	2.89	2.65	3.17	2.66	2.93	2.65	2.59	2.49	3.04	2.79
Li-H	2.00	1.85	2.17	1.86	2.01	1.86	1.84	1.78	2.10	1.93
C1-H	1.52	1.53	1.50	1.53	1.52	1.53	1.55	1.54	1.55	1.55
C3-H	1.38	1.37	1.40	1.38	1.37	1.37	1.34	1.35	1.35	1.36
C3-H-C1	165.7	169.6	165.2	169.3	163.5	169.4	168.6	171.3	165.1	169.2
C1-Li-C2	135.7	138.9	129.7	138.8	129.3	139.3	133.8	137.8	136.8	141.9
ArH-C_2HLi[b]	50.7	57.0	32.9	56.2	56.6	56.7	70.4	68.7	48.7	54.5

bond/angle	**K**	**L**	**M**	**N**	**O**	**P**	**Q**	**R**	**S**	**T**	**U**
Li-N	2.12	---	---	---	2.10	---	---	---	---	---	---
Li-O	---	2.10	2.04[c]	2.03[c]	---	2.11	---	---	---	---	---
Li-C3	2.67	2.59	3.10	3.08	3.11	2.85	2.91	2.88	2.38	2.40	2.77
Li-F	---	---	---	---	---	---	2.17	2.18	---	---	2.21
Li-H	1.90	1.84	2.23	2.21	2.14	1.97	2.11	2.09	1.74	1.76	2.01
C1-H	1.60	1.59	1.53	1.53	1.55	1.55	1.59	1.58	1.51	1.53	1.54
C3-H	1.31	1.32	1.38	1.38	1.32	1.35	1.32	1.33	1.39	1.37	1.36
C3-H-C1	164.0	166.6	173.0	172.8	165.3	168.6	167.2	169.5	176.4	170.6	172.6
C1-Li-C2	134.8	138.4	137.2	136.8	139.1	142.3	141.6	144.1	142.2	141.9	138.7
ArH-C_2HLi[b]	57.7	54.2	61.7	65.2	38.1	48.7	16.3	21.8	99.2	88.3	80.8

[a]See Section **XV**-B for atom numbering. [b]Angle between C_2HLi and ArH planes. [c]Li-OMe interaction.

XVI. (cont.) Selected bond lengths (Å) and angles (deg) for monomer- and dimer-based transition structures **V**-**UU**.[a]

bond/angle	**V**	**W**	**Y**	**AA**	**BB**	**CC**	**DD**	**EE**	**HH**	**II**
Li-N	2.09	---	---	---	2.10	---	2.09	---	---	---
Li-O	---	2.08	2.08	2.08	---	2.09	---	2.12	2.07[b]	2.05[b]
Li-C3	2.59	2.44	2.45	2.44	2.45	2.35	2.66	2.34	2.46	2.47
Li-H	1.80	1.73	1.73	1.73	1.74	1.70	1.83	1.70	1.80	1.81
C1-H	1.50	1.50	1.50	1.50	1.50	1.49	1.52	1.58	1.50	1.50
C3-H	1.39	1.38	1.38	1.38	1.37	1.40	1.37	1.32	1.38	1.40
C3-H-C1	169.3	172.1	172.0	172.0	170.8	174.9	167.8	169.7	168.4	170.6
Li-$\underline{N}$[c]	2.26	2.28	2.28	2.28	2.33	2.33	2.26	2.30	2.20	2.20
ArH-$\underline{N}_2$Li[d]	104.4	94.6	95.4	95.2	102.1	90.0	66.9	86.9	78.3	76.2

bond/angle	**JJ**	**KK**	**LL**	**MM**	**NN**	**OO**	**PP**	**QQ**	**SS**	**UU**
Li-N	2.13	---	---	---	---	---	---	2.07	2.09[e]	1.98[f]
Li-O	2.33[b]	2.16	---	---	---	2.07[b]	---	---	---	---
Li-C3	2.44	2.36	2.48	2.52	2.19	2.43	2.50	2.63	3.43[e]	2.67
Li-F	---	3.72	2.06	2.01	---	---	2.02	---	---	---
Li-H	1.76	1.72	1.80	1.82	1.63	1.80	1.81	1.80	---	1.93
C1-H	1.63	1.61	1.56	1.54	1.48	1.48	1.50	1.50	1.44	1.52
C3-H	1.28	1.30	1.34	1.36	1.42	1.42	1.39	1.38	1.45	1.38
C3-H-C1	166.4	170.1	166.1	167.6	178.5	174.6	172.7	165.9	158.6	168.9
Li-$\underline{N}$[c]	---	2.29	2.15	2.16	2.14	---	2.16	2.25	2.23	---
ArH-$\underline{N}_2$Li[d]	80.4	74.7	79.0	78.2	100.2	73.8	76.5	105.9	94.1	---

[a]See Section **XV**-C for atom numbering. [b]Li-OMe interaction. [c]Av bond distance. [d]Angle between ArH and Li·TMEDA chelate planes. [e]Bond distance to Li2. [f]Bond distance to N1.

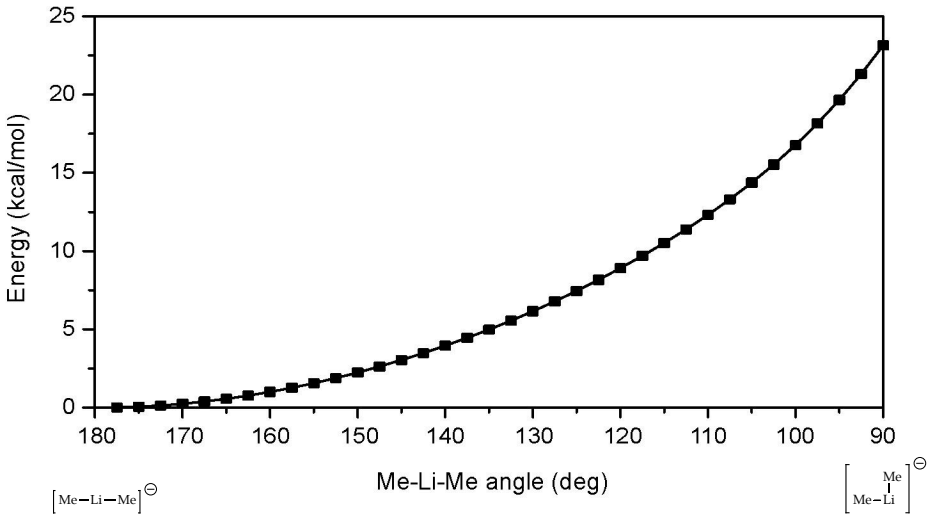

XVII. Potential energy (kcal/mol) as a function of Me-Li-Me angle in relaxed potential energy scan using the B3LYP/6-31G(d) level. The optimum 180° angle was systematically decreased in intervals of 2.5°.